Distribution and ^{129}Xe NMR chemical shifts of Xe_n clusters in the alpha cages of zeolite Ag*A*

Cynthia J. Jameson[a] and Hyung-Mi Lim
Department of Chemistry M/C-111, University of Illinois at Chicago, 845 West Taylor, Chicago, Illinois 60607

(Received 31 March 1997; accepted 11 June 1997)

The distributions and ^{129}Xe NMR chemical shifts of xenon in zeolite Ag*A* have been measured in a series of experiments by Moudrakovski, Ratcliffe, and Ripmeester [Proc. Internat. Zeolite Conference, Quebec, 1995; unpublished]. We carry out grand canonical Monte Carlo (GCMC) simulations of xenon in a rigid zeolite Ag*A* lattice to provide the average Xe_n cluster shifts, and the distributions P_n for comparison with their experiments. The GCMC results for the distributions, the fraction P_n of the alpha cages containing n Xe atoms, are compared with the experimental distributions in 12 samples and the agreement is excellent. The distributions in Na*A* and in Ag*A* are very similar, as can be established from the comparison of the dispersion of the distributions, $\{\langle n^2\rangle - \langle n\rangle^2\}$, and both are different from the idealized hypergeometric distribution, in which the component atoms occupy eight lattice sites per cage under mutual exclusion. The calculated chemical shift increments $[\sigma(Xe_n) - \sigma(Xe_{n-1})]_{AgA}$ are in good agreement with experiment. The differences between these and the increments in zeolite Na*A*, $\{[\sigma(Xe_n) - \sigma(Xe_{n-1})]_{AgA} - [\sigma(Xe_n) - \sigma(Xe_{n-1})]_{NaA}\}$, are fairly small and are in good agreement with experiment. The absolute ^{129}Xe chemical shifts of Xe_n in the alpha cages of Ag*A* are nearly uniformly shifted by about 40 ppm compared to the Xe_n clusters in Na*A*. This is attributed to the Fermi contact shifts arising from the Ag^0 metal atoms that form the linear Ag_3^{2+} complexes that are found within the beta cages of Ag*A*. © *1997 American Institute of Physics.* [S0021-9606(97)50535-6]

I. INTRODUCTION

Most zeolites contain exchangeable cations to balance the anionic framework. Among various cations, silver is of special interest due to the reversible oxidation reduction of silver in zeolites. The light-sensitive hydrated silver zeolite is of interest for its potential to be used for light-write and light-erase materials.[3] Unlike other charge balancing cations in zeolites, silver exists as Ag^+ ion and as Ag^0 to form various sizes of silver clusters. Silver clusters, neutral, or charged, are formed and stabilized in the cavities and the channels of zeolites *A*, *X*, and *Y*, chabazite, mordenite, and rho.[3] Depending on the number, the location, and the oxidation number of silver in the zeolite, the latter provide various chemical environments, which have been studied by ^{129}Xe NMR spectroscopy,[4,5] by electron spin resonance (ESR),[6] and ir spectroscopy,[7] and other methods. For example, ^{129}Xe chemical shifts in the limit of zero loading inside silver zeolite *Y* vary from -50 to 60 ppm relative to the isolated Xe atom.[5] The unusual and unexpected sign of the -50 and -40 ppm shifts observed by Boddenberg, Fraissard, and co-workers[4,5,8] is in contrast to all other ^{129}Xe NMR studies on cation-exchanged Na*X* and Na*Y* zeolites in which Xe exhibits positive chemical shifts relative to the isolated atom.[9] In other Xe in Ag*X* samples with positive ^{129}Xe chemical shifts, the more positive chemical shifts compared to Xe in Na*X* have been attributed to Xe-residual water and Xe–Ag^0 contributions.[4] On the other hand, the unusual negative chemical shifts have been attributed specifically to Xe$\cdots Ag^+$ ion interactions.[4] Why should chemical shifts from interactions of Xe with an Ag^+ ion be different in sign from interactions with Na^+ and other cations? The only other exceptional behavior has been observed in the -70 ppm Xe chemical shift in Cu^+-exchanged Na*Y* where the Cu^+ ions are believed to be in site (III) positions.[10] These are only some of the rather puzzling observations in Ag^+- and Cu^+-exchanged Na*Y* zeolites that await interpretation. In particular, the negative chemical shifts relative to Xe gas are difficult to understand in these cases where Xe is in fast exchange.

^{129}Xe NMR spectra for Xe_n clusters in Ag*A* have been reported by Moudrakovski, Ratcliffe, and Ripmeester.[1,11] These spectra show separate Xe_n peaks, very analogous to the spectra of Xe in Na*A*.[12,13] The same maximum loading (8 Xe atoms per alpha cage) is found, and similar chemical shift increments in going from Xe_n to Xe_{n+1} but the whole spectrum of a progression of Xe_n peaks is shifted by 32–43 ppm to higher chemical shifts compared to the spectra of Xe_n in Na*A*. Two-dimensional exchange spectroscopy (2D-EXSY) studies of Xe in these samples[1] yielded rate constants for cage-to-cage migration that are very similar, although somewhat larger than those reported from 2D-EXSY studies of Xe in Na*A*.[14] The one aspect of Xe in Ag*A* that is different is the $\sim +40$ ppm additional chemical shift of the entire spectrum compared to Na*A*. In all respects but this one, the Xe_n in Ag*A* appears to exhibit the same characteristics as Xe_n in Na*A*. This is very promising, because the quantitative interpretation of Xe_n in Ag*A* by GCMC simulations may provide some insight that can be transferred to the understanding of

[a]Electronic mail: cjj@sigma.chem.uic.edu

some of the puzzling observations of Xe chemical shifts in open network zeolites containing Ag^+ ion. For example, we have found that in order to understand the chemical shifts of Xe in K^+ ion substituted Na*Y*, it was necessary to do the experiments and quantitatively interpret the experimental data of Xe_n in K*A*.[15] In order to quantitatively interpret the Xe chemical shifts in the open zeolite ''Ca*A*,'' it was essential to first interpret the experimental Xe chemical shifts of the Xe_n trapped in the alpha cages of $Ca_xNa_{12-2x}A$, where $x=1$, 2, and 3.[16] GCMC simulations should provide as detailed a description for Xe in the Ag*A* system as it has been able to provide for Xe in Na*A*, and its cation-exchanged varieties, K*A* and $Ca_xNa_{12-2x}A$.[15,16] In this article, we attempt to provide an interpretation of the experimental ^{129}Xe NMR spectroscopy results reported by Moudrakovski, Ratcliffe, and Ripmeester for ''yellow Ag*A*'' samples in which the relative intensities of the Xe_n peaks provide the fraction of alpha cages containing n Xe atoms in 12 samples with $\langle n\rangle_{Xe}$ ranging from 1.45 to 7.55, and the distinct chemical shifts of the Xe_n clusters in the alpha cages of Ag*A* provide information about the environment inside the cages for n Xe atoms.[1,2]

II. METHODS

The GCMC simulation method we use here has been described in detail previously.[15,17] The V(Xe–Xe) potential is a Maitland–Smith functional form fitted to the best Xe–Xe potential for the pair interaction[18]

$$U(r)=\epsilon\left\{\frac{6}{n-6}\,\overline{r}^{-n}-\frac{n}{n-6}\,\overline{r}^{-6}\right\},\quad \overline{r}=r/r_{\min},$$

where n is allowed to vary with r according to $n=13+11(\overline{r}-1)$. The zeolite contribution to the ^{129}Xe chemical shift is assumed to be pairwise sums just like the energy sums, except summing over terms from pair shielding functions rather than potential functions. We use a shielding function $\sigma(^{129}\text{Xe,Xe}\cdots\text{O}_{\text{zeol}})$ which has been derived from *ab initio* quantum mechanical calculations of the ^{39}Ar shielding in the presence of fragments of the *A* lattice, representing 4, 6, and 8 rings of the zeolite.[19] The $\sigma(^{129}\text{Xe,Xe}\cdots\text{Xe})$ shielding function is the same as was used in the previous simulations.[17] The potential functions and the shielding functions are all cut and shifted in the usual manner.[20] The Norman–Filinov technique is used: a displacement step is followed by two steps of particle creation or annihilation attempts.[21] An attempted move is accepted with a probability P_{acc} given by

$$P_{\text{acc}}=\min[1,\exp(-\Delta E/k_BT)],\quad \Delta E/k_BT\leqslant 180$$

$$P_{\text{acc}}=0,\quad \Delta E/k_BT>180$$

and ΔE is calculated from the configurational energy change between the old and new configuration and the imposed value of the configurational chemical potential. Some number of 10^5 cycles were discarded prior to the typically one million cycles constituting the simulation proper, for each choice of chemical potential and temperature. All calculations were done on an IBM RISC/6000 model 560 and model 365. Data were collected as described previously[17,22] to yield distributions (fractions of cages having n Xe atoms), one-body distribution functions, pair distribution functions, and properties of the individual Xe_n clusters. The aspects of the GCMC simulation which are new in this work are described below.

A. Structure of Ag*A*

The structure of Ag*A* is available from several sources, for zeolites which have undergone different pretreatments,[23] different amounts of Ag exchanged starting from Na*A*,[24] different Si/Al ratio,[24] and different amounts of reduced Ag in fully Ag^+-exchanged Ag*A*.[25] When the reduction of Ag^+ is carried out in the dehydration step of the fully Ag^+-exchanged Ag*A*, silver clusters form inside the beta cages. It is known that the extent of Ag^+ cation reduction depends on the dehydration temperature.[3] The yellow color of yellow Ag*A* appears at 378 K due to Ag_3^{++} clusters and the brick-red color of ''red Ag*A*'' appears at more severe dehydration conditions due to formation of larger sizes of clusters.[23,24] X-ray diffraction of the ''Ag*A*-105'' (dehydration at 105 °C, yellow)[23] has Ag^+ located in the 8 ring just as the cation site II in Na*A*, and 6.72 molecules of localized water are found inside the alpha cage. X-ray diffraction of ''Ag*A*-430'' (dehydration at 430 °C, orange color) found no water and one more reduced Ag than Ag*A*-105 so the structure of the former is very similar, in terms of existence of cation sites I, II, and III and no water found, to the structure of $(Ag^+)_{10}(Ag^0)_2Si_{12}Al_{12}O_{47}$, refined by Kim and Seff using single crystal x-ray diffraction.[25] The structure of $(Ag^+)_{88.5}(Ag^0)_{3.5}Al_{12}O_{46.25}$ refined by Kim *et al.*[25] has no cation in the 8-ring window so that Xe is able to be in fast exchange between cages, as was observed in the orange Ag*A* samples of Ripmeester *et al.*[1]

We carried out trial GCMC simulations of Xe in Ag*A* from fully Ag^+-exchanged Na*A* and fully dehydrated (no residual water) and also in Ag*A* fully Ag^+ exchanged and partially dehydrated (with some residual water). Our results reveal that more than 1 and no more than 2 water molecules are needed to keep the maximum occupancy of an alpha cage to the 8 Xe atoms found experimentally and to get the order of magnitude of (Xe_n-Xe_{n-1}) chemical shift increments that was found experimentally by Ripmeester *et al.*[2] Furthermore, there is experimental evidence (observation of ^{129}Xe-^{1}H cross-polarized Xe_n spectra and increase of ^{129}Xe relaxation times upon decrease of residual water in the zeolite) that the Ag*A* used in the experiments by Moudrakovski, Ratcliffe, and Ripmeester have water molecules present inside the alpha cages. Therefore, to represent the yellow Ag*A* samples used by Ripmeester *et al.*, we consider a fully Ag^+ exchanged partially dehydrated Ag*A* based on Gellens' x-ray powder diffraction data on yellow Ag*A*. That is, each alpha cage contains 11 Ag^+ cations and one reduced Ag^0 ion and 2 water molecules inside each alpha cage based on the water positions found by Gellens.[23]

The unit cell composition used in the simulation is

$(Ag^+)_{88}(Ag^0)_8Si_{96}Al_{96}O_{380}\cdot(H_2O)_{16}$. The remaining charge is assumed to be balanced by one hydrogen per alpha cage, but in our simulations the contributions from the hydrogens are neglected. We built a simulation box with two types of alpha cages alternating in the unit cell, satisfying the overall experimental (diffraction) population of Ag. The procedure of selecting the position of Ag^+ cations and water molecules based on x-ray data and their interatomic energies can be summarized as follows. There is much more cation disorder in Ag*A* than in zeolite *A* with other cations. For example, there are three unique positions for site I in the center of the 6 ring and two unique positions for site II. The experimental (diffraction) populations of cation sites is roughly satisfied by using two types of alpha cages (4 ''*A*-type'' alpha cages and 4 ''*B*-type'' alpha cages in a unit cell) with different number of cations, rather than using a single type of alpha cage with some hybrid coordinates considering in and out positions of cation site I and two different positions of cation site II. This is the same reason for choosing two types of cages in building the simulation box for K*A*.[15] The distribution of the Ag ions among the partially occupied equivalent positions provided by the x-ray diffraction data of Gellens *et al.*[23] are assigned by considering the Coulomb energy.

We label the Ag^+ ions with the type of cation site $(I)_a^1$, $(I)_a^2$, and $(I)_b$, or $(II)^1$ and $(II)^2$. First, the Ag^0 and $2Ag(I)_b$ positions are chosen so that they form the experimentally found linear Ag_3^{2+} cluster in the beta cages. The $Ag(I)_b$ in an alpha cage and the $Ag(I)_b$ in the second nearest alpha cage participate to form the linear triatomic Ag_3^{2+} cluster. Ag^0 and $2Ag(I)$ are assumed to be in analogous positions for *A*- and *B*-type alpha cages.

Second, the repulsive coulomb energy of Ag^+ ions is calculated for one unit cell, applying the minimum image convention. All possible configurations of Ag^+ ions with fixed locations of Ag^0 and $2Ag(I)_b$ are considered for *A*-type alpha cages but only certain configurations of Ag^+ ions in *B*-type cage are considered, with the following assumptions to reduce the number of possible configurations: (a) As stated above, Ag^0 and two $Ag(I)_b$ are in the analogous positions in *B*-type alpha cage as in the *A*-type cage so that the Ag_3^{2+} cluster is located in analogous positions in every cage. (b) Of the Ag^+ ions in the cation sites $(II)^1$ and $(II)^2$ located in the 8 ring, one $Ag(II)^1$ and two $Ag(II)^2$, are in analogous positions for two types of cage. (c) The two $Ag(I)_a^2$ positions in the *A*-type cage are assigned and the analogous location is chosen for the single $Ag(I)_a^2$ in the *B* cage.

To find the lowest energy arrangement of ions among the equivalent positions given by x-ray diffraction, we use electrostatic energy calculations. The size of the system for calculations of the electrostatic interactions starts from just one unit cell, with a number of neighboring unit cells which is expanded systematically up to the final calculation of one unit cell surrounded by 26 other unit cells. The ordering of the energy for various Ag^+ ion configurations in the combined *A*-*B* cages is found to be invariant upon increasing the number of cages in the system up to 27 unit cells.

Third, the configuration of water molecules is found based on charge-dipole and dipole-dipole interaction energy. The unlocalized 6.72 H_2O in partially dehydrated Ag*A* is found by x-ray powder diffraction.[23] Using reflectance spectroscopy, from the intensity of the water band with respect to that of the fully hydrated samples, Gellens *et al.* estimated only 1.5 H_2O molecules per unit cell of the yellow form of Ag*A* are left.[23] Considering the maximum number of Xe atoms found in an alpha cage by Ripmeester's experiment, i.e., 8 Xe, our GCMC simulations indicate that the number of H_2O molecules left inside each alpha cage should not exceed 3. The possibility of having 2 or 2.5 (in which case, half of the alpha cages have 2 water molecules and the other half have 3 water molecules) or 3 water molecules inside each alpha cage has been examined in GCMC simulations. The case of having 2.5 or 3 water molecules has been eliminated in our work, since this would result in infrequent incidence of Xe_8 and moreover lead to very large discrepancies in the increments of $(Xe_n - Xe_{n-1})$ chemical shifts compared with the experimental results. Starting from the lowest energy configuration of Ag for a unit cell (with *A*/*B* cages), the minimum energy configuration of two water molecules inside each alpha cage was chosen out of the original 12 equivalent H_2O positions found in the x-ray diffraction.[23] In fact, these 12 water molecule positions are not equivalent anymore after Ag^+ ion locations have been chosen so that cation configuration give the lowest coulomb energy. It turned out that the difference in the charge-charge energies for $Ag^+\cdots Ag^+$ interaction can be smaller than the difference in charge-dipole energies for $Ag^+\cdots H_2O$ in various configurations of Ag^+ so all possible unique configurations of Ag^+ in the above step were again considered here to find out the lowest energy configurations of Ag^+ ions with 2 H_2O in the alpha cage. All possible configurations of H_2O in each unique configuration of Ag^+ in a unit cell (*A* and *B* combined cages) were considered. We found that 2 H_2O in analogous positions in *A*- and *B*-type cages gives lower energies. The lowest energy configuration of two water and 11 Ag^+ and Ag^0 in *A* and *B* cages is found based on the sum of coulomb energy for $Ag^+\cdots Ag^+$, dipole-dipole energy for H_2O-H_2O, and charge-dipole energy for $Ag^+\cdots H_2O$. This configuration is shown in Fig. 1. In this figure, Ag^+ cations are represented by ''+'' symbol except for $Ag(I)_a^1$ which is coordinated to 3 oxygen atoms in the 6 ring and $Ag(I)_b$ which is coordinated to Ag^0 to form the linear Ag_3^{2+} cluster. One Ag^+ cation and two oxygen atoms from H_2O are located in analogous positions for *A* and *B* cage except for one $Ag(I)_a^2$ in the *A* cage in the position of $Ag(I)_a^1$ in *B* cage. There is only one Ag^0 per alpha cage but 4 Ag^0 are shown in Fig. 1 for two alpha cages. The two extra Ag^0 atoms belong to neighboring alpha cages located next to the two alpha cages shown in Fig. 1. The shared extra Ag^0 atoms are shown there to mark the position of the linear cluster of Ag_3^{2+} formed with $Ag(I)_b$ inside two alpha cages shown in the figure. Similarly, there are actually only three cation (II) sites per alpha cage due to sharing with neighboring cages, but 11 sites are shown in the figure for completeness.

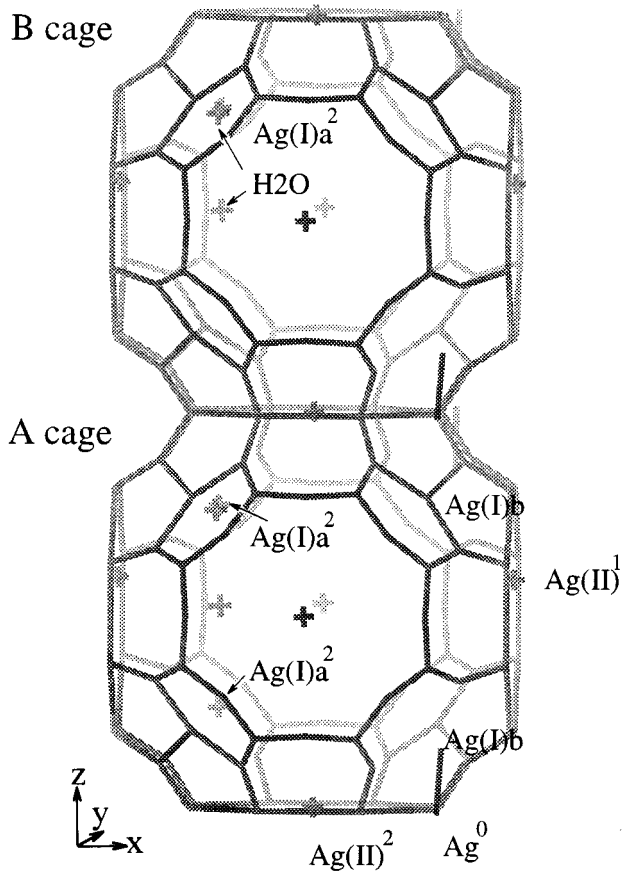

FIG. 1. The configuration of 11 Ag^+ and one Ag^0 and two water molecules in *A*- and *B*-type alpha cages of Ag*A*. Cations are represented by the + symbol except $Ag(I)_a^1$ which is coordinated to 3 oxygen atoms in the 6 ring and $Ag(I)_b$ which is coordinated to Ag^0 to form the linear Ag_3^{2+} cluster. Ag and two oxygen atoms from H_2O are located in analogous positions for *A* and *B* cage except one more $Ag(I)_a^2$ in *A* cage in the position of $Ag(I)_a^1$ in *B* cage. The positions are based on the diffraction results for yellow Ag*A* from Gellens *et al.* (see Ref. 23).

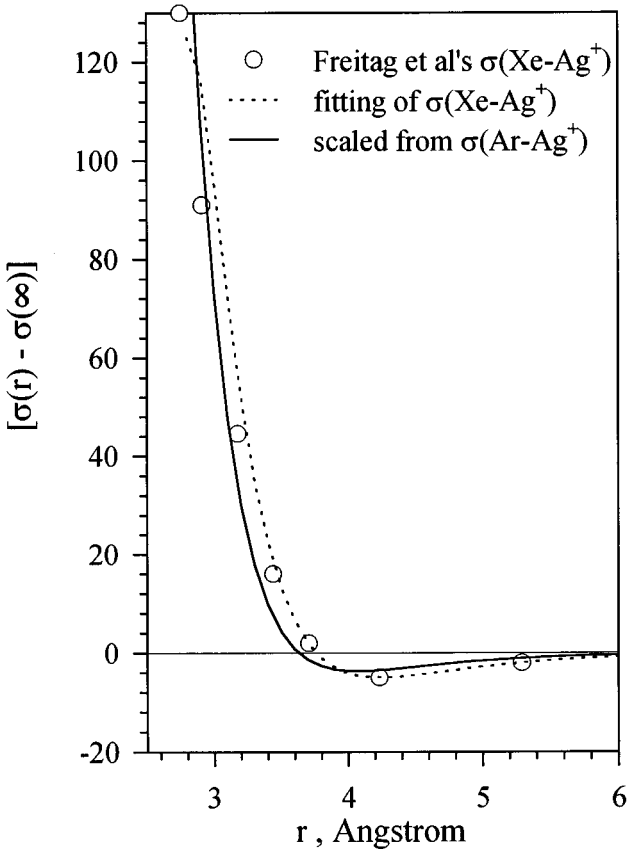

FIG. 2. The ^{129}Xe shielding function of $Xe–Ag^+$ scaled from the ^{39}Ar shielding function obtained from fitting of *ab initio* values of ^{39}Ar shielding for $Ar–Ag^+$ is compared with the shielding function obtained from the fitting of Freitag's *ab initio* values for Xe shielding of $Xe–Ag^+$ (see Ref. 26).

B. Shielding functions for Xe–Ag*A*

The intermolecular chemical shifts of ^{129}Xe in the Xe_n clusters inside the alpha cages of Ag*A* are calculated as pairwise sums of Xe–O shielding contributions from O in the zeolite framework and O in the water molecules, the $Xe–Ag^+$ contributions, and the Xe–Xe contributions. The shielding function $\sigma(Xe–O_{zeol})$ used here is the same as in previous work,[15] which was based on *ab initio* calculations of rare gas atom shielding function in the presence of a zeolite fragment.[19] The shielding contribution from the O atoms of H_2O were considered to be the same as for O atoms in the framework and the contributions of H atoms in H_2O to Xe shielding are neglected. Consistent with this, the contributions from the charge-balancing hydrogens in the zeolite framework are neglected. There is a $\sigma(Xe–Ag^+)$ shielding function in the literature, shown in Fig. 2 calculated using the individual gauge for localized orbitals (IGLO) method.[26] The peculiar shape of this function prompted us to do *ab initio* calculations for comparison. Since the Ag neutral atom basis set but not the Ag^+ ion basis set is available from the handbook, the ion basis set was made from the given basis set of Ag atom[27] by deleting the basis orbital describing $5s$. The validity of obtaining a suitable ion basis by deleting the outermost *s* function was checked by comparing the ^{39}Ar shielding calculated for $Ar–Na^+$ and $Ar–Rb^+$ using the optimized ion basis set for the Na^+ and Rb^+ cations with the ^{39}Ar shielding calculated using an ion basis set made up by deleting the outer *s* orbital of the atom basis set. The difference was negligible. Thus we carried out *ab initio* calculations of the ^{39}Ar shielding as a function of $Ar–Ag^+$ distance, using the gauge-including atomic orbitals (GIAO) method with a 6-311G** basis set for Ar and a basis set for Ag^+ modified from the Huzinaga basis set of Ag atom by deleting the basis orbital describing the $5s$. The $\sigma(Xe–Ag_{zeol})$ shielding function is obtained by scaling in the usual way from the shielding function of $\sigma(Ar–Ag^+)$. The electronic properties of Xe and Ar used in the scaling are as before.[17] The ionization potential of Ag^+ is 22.5437 eV obtained from *ab initio* calculation for Ag^+ using Koopman's theorem and the $r_0(Ar–Ag_{zeol})$ is assumed to be the same as $r_0(Ar–Ne) = 3.146$ Å. In Fig. 2, the $\sigma(Xe–Ag_{zeol})$ scaled from the $\sigma(Ar–Ag^+)$ is compared with the $\sigma(Xe–Ag^+)$ values reported by Freitag *et al.*[26] at various distances. The scaled shielding function $\sigma(Xe–Ag_{zeol})$ is overall of the same shape

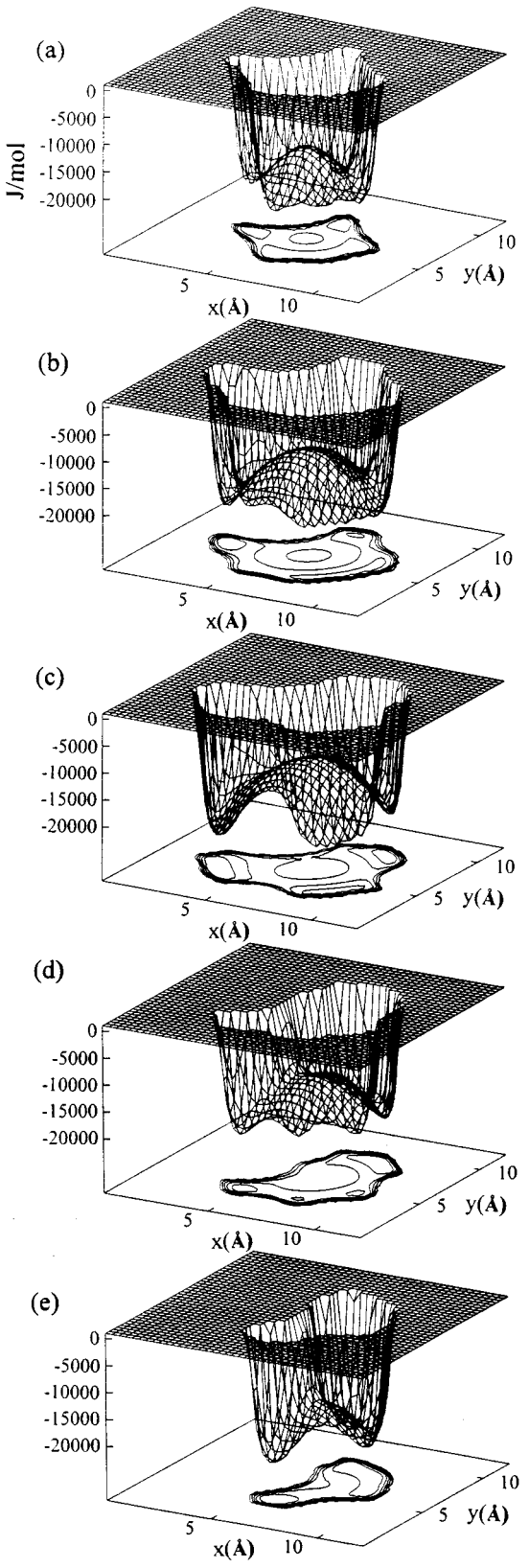

FIG. 3. The potential energy surface of single Xe in the *A* type of Ag*A* cage for selected levels (a) $z=3.541$, (b) $z=4.772$, (c) $z=6.004$, (d) $z=7.235$, and (e) $z=8.467$ Å.

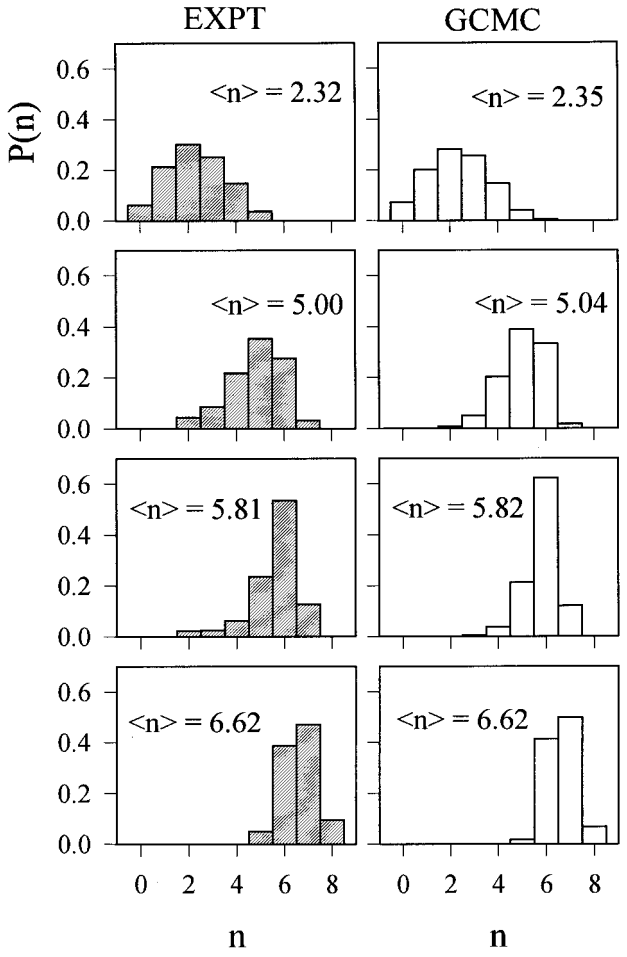

FIG. 4. The distribution of Xe atoms among alpha cages of zeolite Ag*A* in selected samples at 300 K from GCMC simulations are compared with the experimental data from Moudrakovski *et al.* (see Refs. 1 and 2).

as Freitag *et al.*'s shielding function but shifted to smaller r range by about 0.1 Å. The *ab initio* points of $Xe–Ag^+$ shielding from Freitag *et al.*[26] were also fitted to a shielding function which is a sum of r^{-6}, r^{-8}, r^{-10}, and r^{-12} terms for use in GCMC simulations. Although we carried out GCMC simulations with this shielding function, the differences between the results using ours and theirs, all other conditions being kept the same, are not large enough to warrant further comment. The results reported here are those GCMC simulations using the scaled $\sigma(Xe–Ag_{zeol})$ shielding function.

C. Potential function for Xe–Ag*A*

The potential energy of Xe-zeolite interactions is expressed as sums of the pairwise potentials of $Xe–O_{zeol}$, $Xe–O_{H_2O}$, and $Xe–Ag_{zeol}$. Assuming the same effective potential $V(Xe–O_{zeol})$ for all A zeolites, we use the same $V_{LJ}(Xe–O)$ potential function as in previous work[15,17,28] and we use this $V_{LJ}(Xe–O)$ also for the Xe interaction with O atoms of the water molecules. Interactions of Xe with H atom in H_2O were neglected in this work. The estimated potential function for Xe–Ag interaction has $r_0(Xe–Ag_{zeol})$

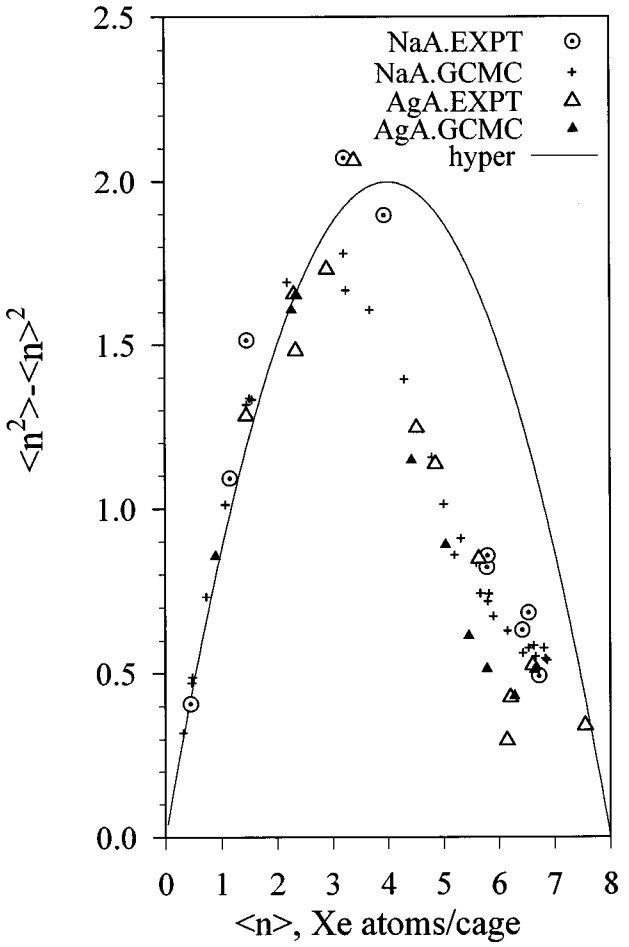

FIG. 5. The dispersion of Xe distributions in Ag*A* from GCMC simulations are compared with the dispersion of the experimental distribution at 300 K from Moudrakovski *et al.* (see Refs. 1 and 2). Also shown are the dispersion of the Xe distribution in Na*A* from GCMC simulations (see Ref. 17) and experiments (see Ref. 12) and the hypergeometric distribution.

smaller than $r_0(\mathrm{Xe–Na_{zeol}})$ and $\epsilon(\mathrm{Xe–Ag_{zeol}})/k_B$ larger than $\epsilon(\mathrm{Xe–Na_{zeol}})/k_B$, based on the ratios of these quantities in the Xe-cation interaction potentials obtained from coupled electron pair approach (CEPA) calculations,[26] or based on the pair potentials obtained by using the Kirkwood–Müller formula.[29] We had previously used the potential $V_{\mathrm{LJ}}(\mathrm{Xe–Na_{zeol}})$ with $r_0=3.676$ Å and $\epsilon/k_B=39.08$ K. Obviously the potential function for the gas phase pair $\mathrm{Xe\cdots Ag^+}$ would have a deeper potential well and a shorter r_0 than the Xe interaction potential with an Ag^+ ion coordinated to oxygen atoms in the zeolite. Starting with the estimated potential energy from CEPA calculations of Xe interacting with Ag^+ ion,[26] or using the Kirkwood Müller formula,[29] the Lennard–Jones potential of $\mathrm{Xe–Ag_{zeol}}$ is adjusted. The extreme limits of parameters found for the potential function of Xe–Ag in the GCMC simulations of Xe in Ag*A* are as follows: $r_0(\mathrm{Xe–Ag})=3.4$ Å seems to be obviously too small and $\epsilon(\mathrm{Xe–Ag_{zeol}})/k_B=120$ K seems to be obviously too large. Any set of potential parameters near $r_0(\mathrm{Xe–Ag})=3.67\pm0.1$ Å and $\epsilon(\mathrm{Xe–Ag})/k_B=50\pm20$ K was found to give reasonable agreement with maximum occupancy of the alpha cages and experimental increments of Xe chemical shifts. We do not have a unique set of parameters for $V_{\mathrm{LJ}}(\mathrm{Xe–Ag_{zeol}})$. In this work, $r_0=3.67$ Å and $\epsilon/k_B=50$ K was chosen for all GCMC simulations of Xe in Ag*A*.

TABLE I. Experimental Xe_n chemical shifts and increments of Xe_n chemical shifts in Ag*A*, ppm at 300 K (see Ref. 2), are compared with experimental Xe_n chemical shifts and increments of Xe_n chemical shifts in Na*A* (see Ref. 12).

	$\delta(\mathrm{Xe}_n)$		$\delta(\mathrm{Xe}_n)-\delta(\mathrm{Xe}_{n-1})$	
	Ag*A*	Ag*A* − Na*A*	Ag*A*	Ag*A* − Na*A*
Xe_1	111.1	36.3		
Xe_2	127.9	35.6	16.8	−0.7
Xe_3	145.8	34.1	17.9	−1.5
Xe_4	165.5	32.3	19.7	−1.8
Xe_5	190.9	32.5	25.7	0.5
Xe_6	219.8	36.4	28.9	3.8
Xe_7	270.5	42.2	50.7	5.6
Xe_8	315.9	43.6	45.4	1.7

III. RESULTS

The potential energy surface for a single Xe atom inside an *A*-type cage is shown in Fig. 3. The corresponding figure for the *B*-type cage is very similar and is not shown here. The potential energy surface of a single Xe atom inside the alpha cage of Ag*A* has an unsymmetrical shape due to the excluded volume made by the presence of two water molecules inside the alpha cage located at (3.057 94, 9.25 706, 6.1575 Å) and (3.057 94, 6.1575, 9.257 06 Å). In addition, there is the excluded volume from one $\mathrm{Ag(I)}_a^2$ ion displaced into the *B*-type alpha cage and the two $\mathrm{Ag(I)}_a^2$ ions in the *A*-type cage. As shown in the potential energy surfaces in Fig. 3, the additional $\mathrm{Ag(I)}_a^2$ ion located inside the *A*-type alpha cage excludes as large a space at level $z=3.541$ Å as the water molecules do. In the *B*-type cage, the volume excluded by the $\mathrm{Ag(I)}_a^1$ ion in the same 6 ring can be seen at the same level.

The distribution of Xe atoms among the alpha cages of Ag*A* obtained from the GCMC simulations at four different Xe loadings at 300 K are plotted in Fig. 4. These and the other eight samples not shown are in good agreement with Ripmeester's experimental distribution of Xe atoms in Ag*A*,

TABLE II. The Xe–O, $\mathrm{Xe–Ag^+}$, and Xe–Xe contributions to ^{129}Xe chemical shifts of Xe_n in the alpha cages of Ag*A* from GCMC simulations.

	$\mathrm{Xe–O_{zeol}}$	$\mathrm{Xe–O_{H_2O}}$	$\mathrm{Xe–Ag_{zeol}}$	Xe–Xe	$\mathrm{Xe–Ag^0}$ estimated
Xe_1	60.6	6.1	6.3	0	38.1
Xe_2	61.0	6.4	6.3	13.7	40.5
Xe_3	61.9	6.7	6.2	29.3	41.7
Xe_4	63.4	7.3	6.0	46.4	42.5
Xe_5	66.3	7.8	5.8	65.4	45.5
Xe_6	69.6	8.2	5.5	87.5	49.1
Xe_7	80.8	8.2	3.7	129.1	48.7
Xe_8	89.5	9.0	2.2	171.0	44.2

TABLE III. Comparison of the Xe–O, Xe cation, and Xe–Xe contributions to Xe_n in Ag*A* with chemical shifts in Na*A*, from GCMC simulations.

	$Xe–O_{zeol}$ Ag*A* − Na*A*	$Xe–M_{zeol}$ Ag*A* − Na*A*	Xe–Xe Ag*A* − Na*A*
Xe_1	2.2	−11.6	0
Xe_2	2.2	−11.7	−1.5
Xe_3	2.2	−11.9	−2.4
Xe_4	2.4	−12.3	−4.0
Xe_5	1.5	−12.8	−7.8
Xe_6	1.3	−13.4	−10.6
Xe_7	4.2	−15.7	−3.6
Xe_8	6.4	−17.6	−0.7

derived from the relative intensities of the Xe_n peaks in their ^{129}Xe NMR spectra.[1] The dispersion of the Xe distribution, $\{\langle n^2\rangle_{Xe} - \langle n\rangle^2_{Xe}\}$, in Ag*A* at 300 K from experimental data of Ripmeester *et al.* and from our GCMC simulations are plotted in Fig. 5 to compare with the distribution of Xe atoms among the alpha cages of Na*A* and also with that predicted from the hypergeometric distribution model. The hypergeometric distribution is added for comparison, since it has been established that this model distribution can reasonably reproduce the experimental distribution of Xe in alpha cage of Na*A* in samples at low to medium Xe loading but can deviate significantly at high loadings.[12,13] We see in Fig. 5 that the dispersion of the experimental distributions of Xe atoms among the alpha cages of Na*A* and Ag*A* are very similar. Both deviate significantly from the strictly statistical hypergeometric model in the same way. In addition, we see that the distributions obtained from GCMC simulations are in good agreement with the experimental distributions in a general way (as described by the dispersion). There appears to be a small difference in the dispersion of the experimental Xe distributions in Na*A* and Ag*A*, toward smaller dispersions in Ag*A* at high Xe loadings, although it is not clear whether this is real outside the experimental uncertainties.

The experimental Xe_n chemical shifts in Ag*A* are compared with Xe_n in Na*A* in Table I. The ^{129}Xe chemical shifts of Xe_n inside the alpha cages of Ag*A* obtained from the GCMC simulations are given in Table II. The separate contributions of $Xe–O_{zeol}$, $Xe–O_{H_2O}$, Xe cation, Xe–Xe, and the estimated contribution of $Xe–Ag^0$ are shown in Table II. A comparison with the separate contributions to the chemical shifts of Xe_n in Na*A* is shown in Table III. The GCMC simulations give only Xe_n chemical shifts composed of $Xe–O_{zeol}$, $Xe–O_{H_2O}$, $Xe–Ag_{zeol}$, and Xe–Xe contributions, and the difference between the absolute shielding from GCMC and the experiment (or the chemical shifts relative to free Xe atom) is attributed to $Xe–Ag^0$ contribution, in the magnitude of 38–49 ppm.

The chemical shift increments in Ag*A* from GCMC simulations is compared with that from experiment in Fig. 6. These increments are in reasonable agreement with experiment. We can also compare the difference of chemical shift increments between Ag*A* and Na*A* obtained from GCMC simulations and experiment. Here, only the qualitative feature, that the sign changes from (−) to (+) in going to larger size of clusters, is reproduced from GCMC simulations, as shown in Fig. 7. These are fairly small numbers, so we can not expect much better agreement, given the approximate potential functions used here.

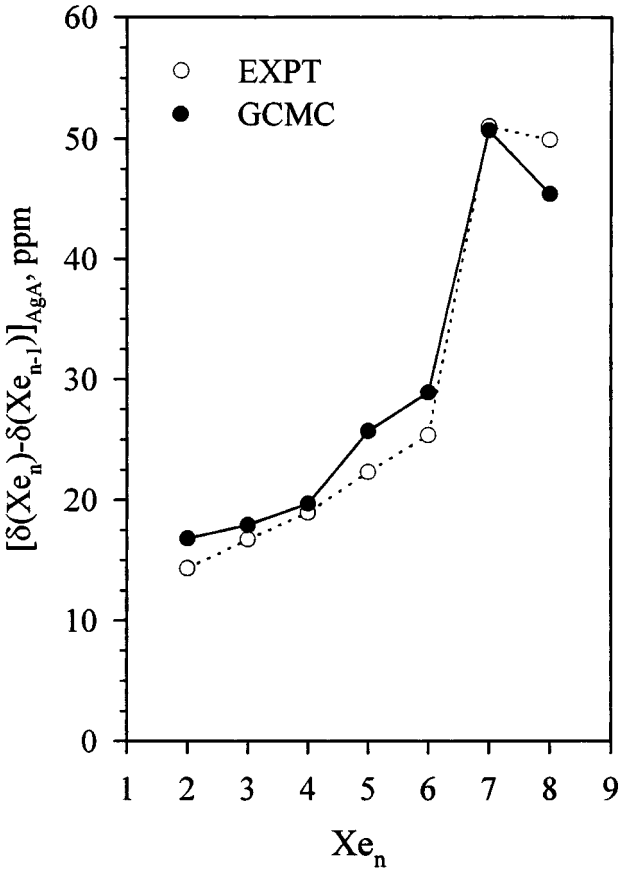

FIG. 6. The chemical shift increments for Xe_n in Ag*A* at 300 K from GCMC simulations are compared with the experimental data from Moudrakovski *et al.* (see Ref. 2).

The larger chemical shifts of Xe_n in Ag*A* compared to Na*A* is partly due to the water molecules inside the alpha cage in Ag*A*, but the water contributions are far too small to account for the 32.3–43.6 ppm difference. The number of H_2O molecules per alpha cage in Ag*A* can be estimated to be no more than 3 even without the aid of GCMC simulations, due to maximum size of Xe_n cluster observed in Ag*A* being Xe_8. In fact from GCMC simulations, the Xe–O contributions coming from the H_2O molecules is 6.1–9.0 ppm for $Xe_1 - Xe_8$, with the larger contribution for the larger size of Xe_n clusters. The slightly larger Xe–O contributions to the Xe_n chemical shifts in Ag*A* compared to that in Na*A* is related to the effectively slightly larger Ag*A* cage, which also results in a slightly smaller Xe–Xe contribution in Ag*A* than in Na*A*, as shown in Table III. The chemical shift difference caused by the small difference in cage size is small, as can be expected from finding the same maximum number (Xe_8) in both Na*A* and Ag*A*.

What about the Xe-cation contribution? The Xe-cation contribution to the Xe_n chemical shifts is much smaller for

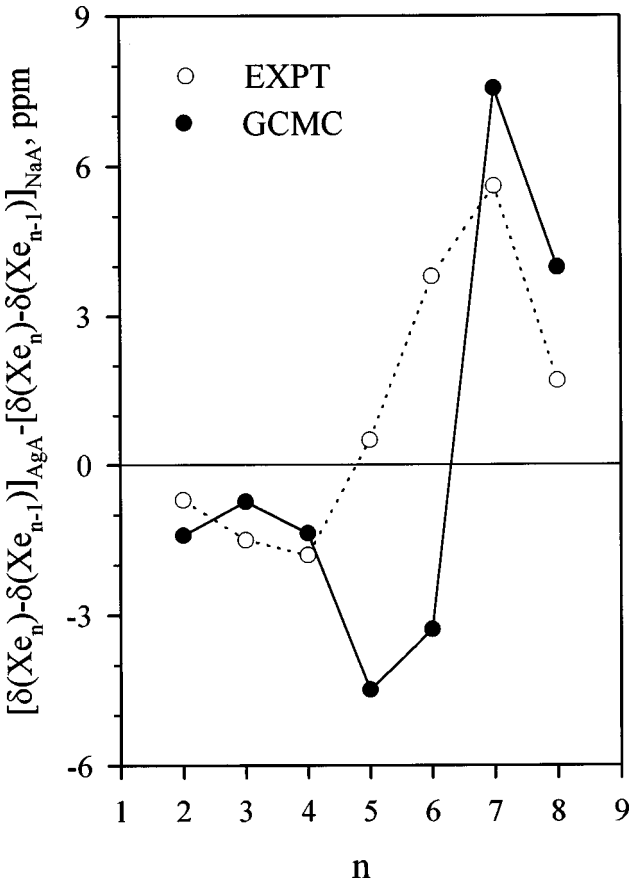

FIG. 7. The difference in the chemical shift increments between Ag*A* and Na*A* at 300 K from GCMC simulations are compared with the experimental data from Moudrakovski *et al.* (see Ref. 2).

$Xe–Ag^+$ ion than for $Xe–Na^+$ (see Table III), as can be expected from a direct comparison of shielding functions, $\sigma(Xe–Na_{zeol})$ and $\sigma(Xe–Ag_{zeol})$. Intermolecular shielding functions have been shown[30–32] to have the form of the shielding function for $Xe–Ag^+$ ion in Fig. 2. That is, relative to the isolated atom, the shielding is zero at infinite separations, then becomes negative as the intermolecular distance decreases, reaches a minimum and then increases again, heading toward the positive shielding of the united atom limit at very short distances. For all the rare gas—other systems previously investigated, the minimum in the shielding function occurs at distances *much much shorter* than the r_0 of the intermolecular potential energy function.[30–32] Thus, even at very high temperatures, the regions of positive intermolecular shielding are not sampled, leading to intermolecular shifts that are deshielding relative to the isolated system (i.e., always positive intermolecular chemical shifts for rare gas nuclei). In contrast, the calculated shielding function $\sigma(Xe–Ag^+)$ shown in Fig. 2 has its minimum at a distance *greater* than the r_{min}=3.04 Å of the $V(Xe–Ag^+)_{CEPA}$ potential energy function reported by Freitag *et al.*[26] and reaches a positive shielding value at 3.7 Å! The $Xe–Ag^+$ chemical shift contribution is smaller than $Xe–Na^+$ but not negative (see Table II), which means the negative chemical shift (that is, positive shielding) portion of the $Xe–Ag_{zeol}$ shielding function at small separations (Fig. 2) does not overwhelm the positive chemical shift portion in the averaging of Xe_n chemical shifts in yellow Ag*A*. In Ag*A*, the cation contribution is actually decreasing with increasing size of Xe_n clusters (see Table II), which is quite different from the case of all contributions (Xe–O, Xe cation, Xe–Xe) to the chemical shift of Xe_n in Na*A*, and quite different from all the other contributions in Ag*A*. This is to the due to the unique location of the shielding minimum in the $\sigma(Xe–Ag_{zeol})$ shielding function relative to the $V(Xe–Ag)$ potential minimum, leading to a positive Xe chemical shift relative to the isolated Xe atom at all distances less than 3.7 Å from Freitag's work,[26] or at all distances less than 3.6 Å from our work.

IV. DISCUSSION

The difference of 35–45 ppm in the absolute chemical shift of Xe_n clusters from GCMC simulations compared to experiment is attributed here to the presence of one Ag^0 inside each beta cage. The estimated magnitude of the $Xe–Ag^0$ contribution in Table II is obtained by subtracting GCMC chemical shifts of Xe_n from the experimental chemical shifts of Xe_n. The 35–45 ppm larger shift is consistent with the 60 ppm larger chemical shifts found for Xe in Ag*X* (after reduction at 100 or 300 °C) compared to Xe in Na*X*,[4,33] which had been attributed to Ag^0 sites in the reduced Ag*X* zeolite. A strong metal–xenon interaction is hinted at in these articles, but neither the number of Ag^0 atoms nor their locations are identified. There may well be a strong $Xe–Ag^0$ interaction energy, but the x-ray diffraction data show the Ag^0 atoms inaccessible to the Xe in the alpha cage by being in the center of the linear Ag_3^{2+} clusters in the beta cages. Thus, only the ends of the linear Ag_3^{2+} clusters are accessible to the Xe atoms. How then do we account for the 35–45 ppm shifts observed? We believe the unpaired electron shared by these three Ag^+ ions can be expected to be somewhat delocalized over all three rather than localized at the center Ag. Thus, the Xe atom will experience the effects of the unpaired electron. The effects of the unpaired electrons in O_2 and NO on Xe, over and above the usual chemical shift second virial coefficient of Xe interacting with a diamagnetic molecule, have been previously established.[34–36] In addition to the bulk magnetic susceptibility effects, which gives a positive chemical shift contribution in a cylindrical sample parallel to the magnetic field when unpaired electrons contribute to the susceptibility, there is also some contribution from the Fermi contact interaction, leading to a highly temperature dependent positive chemical shift larger than that found for a diamagnetic collision partner with about the same electric dipole polarizability. This explanation has been advanced to interpret the experimental temperature behavior of the density coefficient of the Xe chemical shift in $Xe–O_2$ mixtures and Xe–NO mixtures.[34–36] The effects of the Fermi contact interaction have been estimated theoretically in terms of the same mechanisms, overlap, and exchange, that are generally responsible for intermolecular shifts of rare gas atoms in a calculation of Fermi contact shifts in Xe and NO by Buck-

TABLE IV. The Xe–O, Xe–Ag^+, and Xe–Xe contribution to ^{129}Xe chemical shift *increments* in Ag*A* alpha cage, compared with Xe chemical shift increments in Na*A* cage, all from GCMC simulations.

	Ag*A*				Ag*A* − Na*A*		
	$Xe–O_{zeol}$	Xe–Ag	Xe–Xe	$Xe–O_{H_2O}$	$Xe–O_{zeol}$	Xe–M	Xe–Xe
Xe_2-Xe_1	0.4	0.0	13.7	0.3	0.0	−0.1	−1.5
Xe_3-Xe_2	0.9	−0.1	15.6	0.3	0.0	−0.2	−0.9
Xe_4-Xe_3	1.5	−0.1	17.1	0.6	0.2	−0.3	−1.6
Xe_5-Xe_4	3.0	−0.3	19.0	0.5	−0.8	−0.6	−3.8
Xe_6-Xe_5	3.2	−0.3	22.1	0.4	−0.3	−0.6	−2.8
Xe_7-Xe_6	11.2	−1.8	41.6	0.1	2.9	−2.3	7.0
Xe_8-Xe_7	8.7	−3.3	42.0	0.8	2.2	−3.4	4.4

ingham and Kollman.[37] We believe the 35–45 ppm shifts in Ag*A* to be largely due to the Fermi contact shift.

The small difference in the chemical shift *increments* in Ag*A* and Na*A* in Table I can be explained by GCMC simulations. This case is different from Xe_n in K*A* compared to Xe_n in Na*A*.[15] In K*A*, the larger chemical shifts of Xe_n compared to Na*A* are due to the larger shielding of $\sigma(Xe–K_{zeol})$ combined with a deeper potential well of $V(Xe–K)$. The monotonically larger increments of Xe chemical shifts in K*A* compared to Na*A* are due to the larger excluded volume in K*A* mainly from the in-out placement of the K^+ ions in the alpha cages. Thus, the difference between the increments in K*A* and Na*A* are monotonically positive and increasing with cluster size: 1.4, 1.9, 4.2, and 9.9 ppm. Simulations in K*A* did provide this trend.[15] The Xe_n in Ag*A* show only larger chemical shifts with very similar increments to those found in Na*A*. The difference between the increments in Ag*A* and Na*A* are −0.7, −1.5, −1.8, and 0.5 ppm (and 3.8, 5.6, and 1.7 ppm for the larger Xe_n clusters that were not observed in K*A*). The GCMC simulations do provide the correct qualitative trend here: negative changing over to positive, with an *S* shape, as seen in Fig. 7, although the agreement is not quantitative. Finally, Table IV provides the analysis of the different contributions to the (Xe_n-Xe_{n-1}) incremental chemical shifts. We see that, just as in Na*A*, the increments are dominated by the Xe–Xe contributions which are rapidly increasing with the shorter Xe–Xe distances for averaging of the shielding as the cage gets more crowded. The contributions of $Xe\cdots O_{zeol}$ to the chemical shift increments is small and increasing slightly as the cage gets more crowded. The $Xe\cdots Na^+$ contributions to the increments in Na*A* behave like the $Xe\cdots O_{zeol}$ increments, small and increasing slightly as the cage gets more crowded. But in Ag*A*, the Xe···Ag contributions to the increments are negative and becoming slightly more negative as the cage gets more crowded. The peculiar position of the minimum shielding in the Xe···Ag shielding function relative to the r_0 of the potential function is responsible for this. In other shielding functions, the distances in the region where the shielding function changes sign are very short, and these distances are never sampled at ordinary temperatures, thus, no contributions to the intermolecular shift of unusual sign are observed. In contrast, the ^{129}Xe shielding relative to the isolated Xe atom in the Xe···Ag system changes sign at separations which are sampled at ordinary temperatures. As the cage gets more crowded, contributions of unusual sign become more important. Nevertheless, they are small, as seen in Table IV and do not alter to a great extent the trends in the total Xe_n shifts which are dominated by the Xe–Xe contributions. Therefore, the general behavior of the total Xe_n chemical shifts and their increments in Ag*A* look just like those of Xe_n in Na*A*.

It is interesting that observing the ^{129}Xe NMR spectrum of Xe_n in Ag*A* under magic angle spinning improves the resolution well enough to observe that the Xe_7 and Xe_8 clusters are present in two distinct peaks each, one smaller than the other.[1,2] This indicates one of two things: that there are at least two distinct types of alpha cages in yellow Ag*A* (perhaps with small differences in the locations of the Ag^+ ions) and only in the very crowded cages can these small differences be probed by the Xe nuclei, or that the large number of Xe atoms in the crowded cages induce these alpha cages to distort away from the structure of half empty or empty cages. Incidentally, even in this experimental aspect, the Xe_n in Ag*A* behaves similarly to Xe_n in Na*A*, in which this behavior was observed for the first time.[38]

There are some approximations used in this work that could be improved upon. In this work, we have not separated out the contributions to the polarization of Xe by the zeolite; the $V_{LJ}(Xe–O_{zeol})$ and the $V_{LJ}(Xe–Ag_{zeol})$ we used are effective potentials which represent the totality of Xe-zeolite interactions, including the induction terms. On the basis of GCMC simulations of Xe_n in Na*A* using both explicit and implicit induction contributions, we expect that the distributions and chemical shifts from simulations using explicit Xe polarization terms in Ag*A* will be very similar to the ones found here. We could have done *ab initio* calculations on Ag*A* zeolite fragments (similar to those we carried out for Na*A*, K*A*, and Ca*A* fragments) in order to obtain the $\sigma(Xe\cdots Ag_{zeol})$ shielding function, instead of using the more approximate $Xe\cdots Ag^+$ model. In simulations of Xe in Na*A*, using the $Xe\cdots Na^+$ model for the $\sigma(Xe\cdots Na_{zeol})$ shielding function tends to lead to larger Xe···Na contributions to the Xe_n shielding than using the $\sigma(Xe\cdots Na_{zeol})$ shielding function from the zeolite Na*A* fragment calculations.[15] On this basis, we expect that using the $Xe\cdots Ag^+$ model leads to $\sigma(Xe\cdots Ag_{zeol})$ contributions that are likewise less accurate,

but not necessarily in the same way because of the shape of the $\sigma(Xe\cdots Ag^+)$ function.

With respect to the negative Xe chemical shift puzzles in Ag*Y* and Ag*X*,[4] unusual negative average Xe chemical shifts could arise from the $Xe–Ag^+$ shielding functions shown in Fig. 2, but this would require that the Xe atom take configurations which are at all times shorter than 3.7 Å from the Ag^+ ion. Since Xe atoms in a zeolite are physisorbed rather than chemisorbed, the larger fraction of configurations with Xe···Ag distances greater than 3.7 Å, giving positive chemical shift contributions, could easily overwhelm the negative contributions coming from configurations with Xe···Ag distances less than 3.7 Å. The positive chemical shift contributions from the more numerous $Xe\cdots O_{zeol}$ interactions persist. Therefore, unless there exists some unusually strong adsorption site separated from other possible Xe locations by high energy barriers, it is difficult to imagine the $Xe\cdots Ag^+$ shielding functions in Fig. 2 giving negative average Xe chemical shifts in zeolites.

V. CONCLUSIONS

The experimental results of Moudrakovski, Ratcliffe, and Ripmeester for the Xe NMR spectra of Xe in yellow Ag*A*[1,2] has been simulated here using the grand canonical Monte Carlo method. The $Xe–Ag_{zeol}$ shielding function, $\sigma(Xe–Ag_{zeol})$, is modeled from the *ab initio* calculations of ^{39}Ar shielding function in the $Ar\cdots Ag^+$ system, scaled up to the ^{129}Xe shielding function using fundamental atomic properties. This scaled function is very similar to that reported by Freitag *et al.* from *ab initio* calculations on the $Xe\cdots Ag^+$ ion system. This $\sigma(Xe–Ag_{zeol})$ shielding function, and the $\sigma(Xe\cdots Xe)$ and the $\sigma(Xe\cdots O_{zeol})$ shielding functions used in our previous work, averaged over the configurations generated in GCMC simulations, provide the average shielding of Xe_n clusters in Ag*A*. The number of water molecules remaining in the alpha cages of yellow Ag*A* are estimated to be ~ 2, from the maximum occupancy (8 Xe atoms) obtained experimentally. The $(Xe_n - Xe_{n-1})$ ^{129}Xe chemical shift increments in Ag*A* are well reproduced by the simulations. These increments are similar to those found in the cages of Na*A*, but smaller for the small clusters and larger for the larger clusters, which trend is also qualitatively reproduced by the GCMC simulations. The only part of the Xe_n behavior in Ag*A* that is significantly different from Xe_n in Na*A* is the difference in the absolute chemical shifts of Xe_n in Ag*A* compared to the corresponding Xe_n in Na*A* of about $+40$ ppm. We have attributed this to the unpaired electron effects (Fermi contact shifts) arising from interactions between Xe and the ends of the Ag_3^{2+} linear clusters located in the beta cages and projecting into the alpha cages where the Xe_n are found. This positive shift is of the correct sign to be expected of a Fermi contact shift.

The present work indicates that the Xe atoms interacting with Ag^+ ions do not give unusual average chemical shifts, that the distribution and chemical shift behavior of Xe_n in Ag*A* is not unusual in comparison to that of Xe_n in Na*A*. The unusual negative chemical shifts reported for Xe in fast exchange in zeolite Ag*Y* or Ag*X*[4,5,8] remain a puzzle and can not be attributed merely to strong interactions between Xe and Ag^+ ions in the zeolite as originally proposed, since those reports of unusual shifts can not be reconciled with the very conventional behavior of Xe_n in Ag*A*.

ACKNOWLEDGMENTS

This research has been supported by the National Science Foundation (Grant No. CHE95-28066). We thank Igor Moudrakovski, Chris Ratcliffe, and John Ripmeester for generously providing us with their data prior to publication.

[1] I. L. Moudrakovski, C. I. Ratcliffe, and J. A. Ripmeester, in Proceedings of the International Zeolite Conference in Quebec City, 1995.
[2] I. L. Moudrakovski, C. I. Ratcliffe, and J. A. Ripmeester (unpublished).
[3] T. Sun and K. Seff, Chem. Rev. **94**, 857 (1994).
[4] A. Gedeon, R. Burmeister, R. Grosse, B. Boddenberg, and J. Fraissard, Chem. Phys. Lett. **179**, 191 (1991).
[5] R. Grosse, R. Burmeister, B. Boddenberg, A. Gedeon, and J. Fraissard, J. Phys. Chem. **95**, 2443 (1991).
[6] J. R. Morton and K. F. Preston, Zeolites **7**, 2 (1987).
[7] M. D. Baker, J. Godber, and G. A. Ozin, J. Phys. Chem. **89**, 2299 (1985).
[8] R. Grosse, A. Gedeon, J. Fraissard, and B. Boddenberg, Zeolites **12**, 909 (1992).
[9] S. B. Liu, B. M. Fung, T. C. Yang, E. C. Hong, C. T. Chang, P. C. Shih, F. H. Tong, and T. L. Chen, J. Phys. Chem. **98**, 4393 (1994).
[10] M. Hartmann and B. Boddenberg, Microporous Mater. **2**, 127 (1994).
[11] J. A. Ripmeester and C. I. Ratcliffe, *Proceedings of the 9th International Zeolite Conference, Montreal 1992,* edited by R. von Ballmoos *et al.* (Butterworth-Heinemann, New York, 1993), pp. 572–578.
[12] C. J. Jameson, A. K. Jameson, R. E. Gerald II, and A. C. de Dios, J. Chem. Phys. **96**, 1676 (1992).
[13] B. F. Chmelka, D. Raftery, A. V. McCormick, L. C. de Menorval, R. D. Levine, and A. Pines, Phys. Rev. Lett. **66**, 580 (1991); **67**, 931 (1991).
[14] R. S. Larsen, J. Shore, K. Schmidt-Rohr, L. Emsley, H. Long, and A. Pines, Chem. Phys. Lett. **214**, 220 (1993).
[15] C. J. Jameson, A. K. Jameson, R. E. Gerald II, and H.-M Lim, J. Chem. Phys. **103**, 8811 (1995).
[16] C. J. Jameson, H.-M Lim, and A. K. Jameson, Solid State Nucl. Magn. Reson. (in press).
[17] C. J. Jameson, A. K. Jameson, B. I. Baello, and H. M. Lim, J. Chem. Phys. **100**, 5965 (1994).
[18] R. A. Aziz and M. J. Slaman, Mol. Phys. **57**, 825 (1986).
[19] C. J. Jameson and H.-M. Lim, J. Chem. Phys. **103**, 3885 (1995).
[20] M. P. Allen and D. J. Tildesley, *Computer Simulation of Liquids* (Clarendon, Oxford, 1987).
[21] G. E. Norman and V. S. Filinov, High Temp. **7**, 216 (1969).
[22] C. J. Jameson, A. K. Jameson, H. M. Lim, and B. I. Baello, J. Chem. Phys. **100**, 5977 (1994).
[23] L. R. Gellens, W. J. Mortier, R. A. Schoonheydt, and J. B. Uytterhoeven, J. Phys. Chem. **85**, 2783 (1981).
[24] L. R. Gellens, W. J. Mortier, and J. B. Uytterhoeven, Zeolites **1**, 11 (1981).
[25] Y. Kim and K. Seff, J. Am. Chem. Soc. **99**, 7055 (1977).
[26] A. Freitag, C. van Wullen, and V. Staemmler, Chem. Phys. **192**, 267 (1995).
[27] S. Huzinaga, *Gaussian Basis Sets for Molecular Calculations* (Elsevier, Amsterdam, 1984).
[28] C. J. Jameson, A. K. Jameson, and H. M. Lim, J. Chem. Phys. **104**, 1709 (1996).
[29] A. V. Kiselev, A. A. Lopakin, and A. A. Shulga, Zeolites **5**, 261 (1985).
[30] C. J. Jameson and A. C. de Dios, in *Nuclear Magnetic Shielding and Molecular Structure*, edited by J. A. Tossell (Kluwer, Dordrecht, 1993), pp. 95–116.
[31] C. J. Jameson and A. C. de Dios, J. Chem. Phys. **97**, 417 (1992).

[32] C. J. Jameson and A. C. de Dios, J. Chem. Phys. **98**, 2208 (1993).
[33] B. Boddenberg and J. Waterman, Chem. Phys. Lett. **203**, 531 (1993).
[34] C. J. Jameson and A. K. Jameson, Mol. Phys. **20**, 957 (1971).
[35] C. J. Jameson, A. K. Jameson, and S. M. Cohen, Mol. Phys. **29**, 1919 (1975).
[36] C. J. Jameson, A. K. Jameson, and S. M. Cohen, J. Chem. Phys. **65**, 3397 (1976).
[37] A. D. Buckingham and P. A. Kollman, Mol. Phys. **23**, 65 (1972).
[38] A. K. Jameson, C. J. Jameson, A. C. de Dios, E. Oldfield, R. E. Gerald II, and G. L. Turner, Solid State Nucl. Magn. Reson. **4**, 1 (1994).